Structural Engineering and Mechanics, *Vol. 65, No. 3 (2018) 263-274*
DOI: https://doi.org/10.12989/sem.2018.65.3.263

Vibration analysis of a multi-span beam subjected to a moving point force using spectral element method

Boseop Jeong[a], Taehyun Kim[b] and Usik Lee[*1]

Department of Mechanical Engineering, Inha University, Inha-ro 100, Nam-gu, Incheon 22212, Republic of Korea

(Received May 20, 2017, Revised December 24, 2017, Accepted December 26, 2017)

Abstract. In this study, we propose a frequency domain spectral element method (SEM) for the vibration analysis of a multi-span beam subjected to a moving point force. This study is an extension of the authors' previous study for a single-span beam subjected to a moving point force, where the two-element model-based SEM was applied. In this study, each span of a multi-span beam is represented by the Timoshenko beam model and the moving point force is transformed into the frequency domain as a series of each stationary point force distributed on the multi-span beam. The span at which a stationary point force is located is represented by two-element model, but all other spans are represented by one-element models. The vibration responses to a moving point force are obtained by superposing all individual vibration responses generated by each stationary point force. The high accuracy and computational efficiency of the proposed SEM are verified by comparing the solutions by SEM with exact analytical solutions by the integral transform method (ITM) as well as the solutions by the finite element method (FEM).

Keywords: multi-span beam; moving point force; vibration response; spectral element method; two-element model; Timoshenko beam model

1. Introduction

In general, moving load problems deal with severe vibrations and instability of the beam-like one-dimensional (1-D) structures subjected to moving loads (forces and masses), which may involve the interaction of moving loads and structural systems. Typical examples of such problems are bridges, railroads, guideways, cableways, and pipelines. Thus, accurate prediction of the dynamic characteristics and responses of such structures has been an important research issue for over a century.

Many analytical solution techniques have been reported since Frýba's monograph (1999). Examples include the integral transform method (ITM) (Frýba 1999), assumed mode method (Lee 1994, Lee 1996), component mode synthesis method (De Salvo *et al*. 2010), dynamic stiffness method (Henchi *et al*. 1997, Kwon *et al*. 1998), expanded dynamic bending deflection (Dmitriev 1977), Fourier series method (Xu and Li 2008, Li and Xu 2009, Tehrani and Eipakchi 2012), Galerkin method (Dmitriev 1974, Dmitriev 1982), generalized moving least square method (Kiani *et al*. 2010), least squares regularization method (Asnachinda *et al*. 2008), modal analysis method (Wang 1997, Wang and Lin 1998, Hong and Kim 1999, Wang and Sang 1999, Ichikawa *et al*. 2000, Dugush and Eisenberger 2002, Johasson *et al*. 2013, Szylko-Bigus and Sniady 2015, Kim *et al*. 2017), mode superposition method (Zhu and Law 1999, Wang et al. 2003, Jiang *et al*. 2004, Chan and Ashebo 2006), modified beam vibration functions method (Zheng *et al*. 1998, Cheung *et al*. 1999), semi-analytic method (Martinez-Castro *et al*. 2006), transfer matrix method (Wu and Dai 1987, Ariaei *et al*. 2011, Ariai *et al*. 2013), and U-transformation and mode method (Cai *et al*. 1988). However, analytical solution techniques are often limited to simple geometries and boundary conditions. Thus, various numerical solution techniques have been developed.

The finite element method (FEM) is one of the most widely used numerical solution techniques by many researchers (Tang and Wang 2002, Lou *et al*. 2012, Lou and Au 2013). However, in spite of its wide applicability, FEM has an important drawback. The shape functions (or interpolation functions) used in FEM are not dependent on the vibration frequency. Thus, to improve the solution accuracy of FEM, a structural member must be discretized into many smaller finite elements that are far smaller than the wavelength of the highest vibration mode. In general, this results in a finite element model with a huge number of degrees of freedom, which requires an excessive computation time.

In contrast to FEM, frequency-dependent dynamic shape functions are used in the frequency-domain spectral element method (SEM). These shape functions are derived from exact free wave solutions that satisfy the governing equations of motion in the frequency domain. Thus, SEM can provide both exact frequency-domain solutions (natural frequencies and modes) and extremely accurate time-domain solutions (time histories of the dynamic responses). This is accomplished by efficiently taking into account as

*Corresponding author, Professor
E-mail: ulee@inha.ac.kr
[a]MSc. Student
E-mail: bsjeong@inha.edu
[b]Ph.D. Student
E-mail: thyunkim@inha.edu

ISSN: 1225-4568 (Print), 1598-6217 (Online)

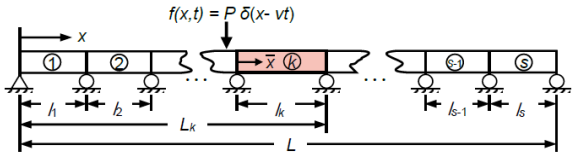

Fig. 1 A multi-span beam subjected to a moving point force

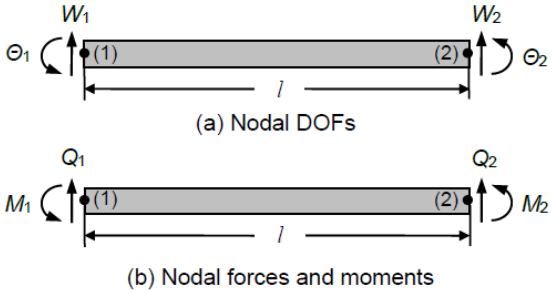

Fig. 2 Spectral element model: (a) nodal DOFs, and (b) nodal forces and moments

many high-frequency wave modes as required by using the fast Fourier transform (FFT) algorithm. Furthermore, due to the use of exactly formulated dynamic shape functions, SEM is shear locking-free and a uniform structural member without any geometrical and material discontinuities or external forces can be represented by a single finite element (one-element model), regardless of its dimensions. This can drastically reduce the problem size and thus the computation time (Lee 2009, Krawczuk *et al*. 2003).

Despite the advantages, only a few researchers have applied SEM to moving load problems. Azizi *et al*. (2012) and Sarvestan *et al*. (2015) applied SEM to the dynamics of continuous beams and bridges subjected to a moving load. They discretized a uniform beam into multiple segments and applied a one-element model to the segment on which a moving load is located. The one-element model commonly in the standard FEM approximately represents a moving load located in a segment as effective nodal forces and moments acting on the two end-nodes of the finite segment. Thus, they could not fully benefit from the advantages of SEM.

Recently, Song *et al*. (2016) applied SEM to the vibration of a single-span Timoshenko beam subjected to a moving point force. They obtained very accurate solutions by representing the moving point force as a series of stationary point forces in the frequency domain and applying a two-element model to the entire span of the Timoshenko beam subjected to each stationary point force. To the best of our knowledge, however, SEM has not been applied to the multi-span beams subjected to moving loads.

Thus, we propose a spectral element analysis method for the vibrations of multi-span beams subjected to a moving point force as an extension of our previous work for single-span beams subjected to a moving point force (Song *et al*. 2016). Based on discrete Fourier transform (DFT) theory, the point force moving on a multi-span beam is transformed into the frequency domain as a series of stationary point forces acting on the multi-span beam simultaneously. The vibration responses are then obtained in the frequency and time domains by superposing all individual vibration responses excited by each stationary point force. To obtain an individual vibration response excited by a stationary point force, the span where the stationary point force is located is represented by a two-element model, where the stationary point force is located at the junction for two finite elements. The high accuracy and computational efficiency of the proposed method are verified by comparison with exact solutions and FEM results.

2. Problem statement

A multi-span beam subjected to a moving point force is shown in Fig. 1. The point moving force has a constant magnitude P and moves at a constant velocity v. The multi-span beam has a length L and it consists of s spans, where l_k (k = 1,2,3, …, s) denotes the length of the kth span. In Fig. 1, x is the global coordinate with an origin at the left-most end of the multi-span beam and $\bar{x}$ is the local coordinate with an origin at the left end of a span. The distance from x = 0 to the right-end of the kth span is defined by

$$L_k = \sum_{e=1}^{k} l_e \ (k = 1, 2, 3, \ldots, s) \tag{1}$$

3. Spectral element model of a uniform span

Based on Timoshenko beam theory, the forced vibrations of a uniform span can be represented by the equations of motion (Lee 2009)

$$\begin{aligned} \kappa GA(w'' - \theta') - \rho A\ddot{w} &= -f(x,t) \\ EI\theta'' + \kappa GA(w' - \theta) - \rho I\ddot{\theta} &= 0 \end{aligned} \tag{2}$$

where $w(x,t)$ and $\theta(x,t)$ are the transverse displacement and the slope due to bending, respectively, and $f(x,t)$ is the external force applied on the span. E is the Young's modulus, G is the shear modulus, ρ is the mass density, A is the cross-sectional area, I is the area moment of inertia, and κ is the shear correction factor of the span. One prime ($'$) and two primes ($''$) denote the first and the second derivatives with respect to x, and two dots ($\ddot{}$) denote the second derivatives with respect to t.

Using DFT theory (Newland 1993), Eq. (2) can be transformed to the frequency domain as follows (Lee 2009)

$$\begin{aligned} \kappa GA(W'' - \Theta') + \omega^2 \rho AW &= -F(x,\omega) \\ EI\Theta'' + \kappa GA(W' - \Theta) + \omega^2 \rho I\Theta &= 0 \end{aligned} \tag{3}$$

where $W(x,\omega)$, $\Theta(x,\omega)$, and $F(x,\omega)$ are the Fourier components of the transverse displacement $w(x,t)$, slope $\theta(x,t)$, and external force $f(x,t)$ at discrete frequency ω.

Following the spectral element formulation procedure described in Chapter 3 of Lee (2009), the frequency-domain spectral element model for a span of length l can be formulated from Eq. (3) in the following form

$$\boldsymbol{S}(\omega, l)\boldsymbol{d} = \boldsymbol{f}(\omega) \tag{4}$$

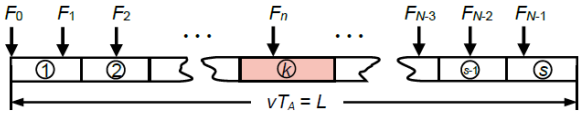

Fig. 3 A series of stationary point forces in the frequency domain when $T = T_A$

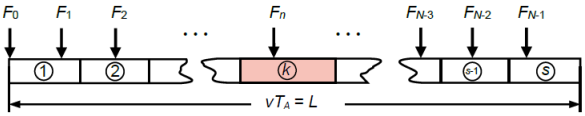

Fig. 4 A multi-span beam subjected to a stationary point force F_n acting on the kth span, where the numbers in parentheses denote the node numbers

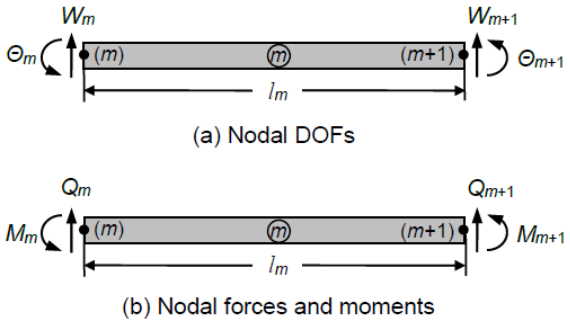

Fig. 5 Nodal DOFs, forces, and moments for the mth span

where $\boldsymbol{S}(\omega,l)$ is the symmetric frequency-dependent 4-by-4 spectral element matrix (or the exact dynamic stiffness matrix). Its components are provided in Appendix A. $\boldsymbol{d}$ and $\boldsymbol{f}$ are the Fourier components of the nodal degrees of freedom (DOFs) and the nodal forces and moments, respectively

$$\begin{aligned} \boldsymbol{d} &= \{W_1 \;\; \Theta_1 \;\; W_2 \;\; \Theta_2\}^{\mathrm{T}} \\ \boldsymbol{f} &= \{Q_1 \;\; M_1 \;\; Q_2 \;\; M_2\}^{\mathrm{T}} \end{aligned} \tag{5}$$

The nodal DOFs (W_i and Θ_i, where i = 1, 2) and the nodal forces and moments (Q_i and M_i, where i = 1, 2) are shown in Fig. 2. Once the nodal DOFs $\boldsymbol{d}$ are obtained for the whole multi-span beam, the displacement fields in a span can be obtained from

$$W(x,\omega) = \boldsymbol{N}_w(x,\omega;l)\boldsymbol{d}, \quad \Theta(x,\omega) = \boldsymbol{N}_\theta(x,\omega;l)\boldsymbol{d} \tag{6}$$

where $\boldsymbol{N}_w(x,\omega;l)$ and $\boldsymbol{N}_\theta(x,\omega;l)$ are 1-by-4 frequency-dependent dynamic shape functions that are already available (Lee 2009).

4. Spectral element analysis for a multi-span beam under a moving point force

4.1 Frequency-domain representation of a moving point force

By using the Dirac delta function, a point force of constant magnitude P that moves at a constant velocity v can be represented by

$$f(x,t) = P\,\delta(x - vt) \tag{7}$$

The moving point force can be transformed in the frequency domain as follow by applying DFT to Eq. (7) with respect to t and applying a discrete representation of a continuous function of x to the DFT result (Song *et al.* 2016)

$$F(x,\omega) = \sum_{n=0}^{N-1} F_n \delta(x - x_n) \tag{8}$$

where

$$F_n = P e^{-i\omega\frac{x_n}{v}} \quad (n = 0,1,\ldots,N-2,N-1) \tag{9}$$

and

$$x_n = vt_n = vn\Delta t = \frac{vnT}{N} \tag{10}$$

where $\Delta t = T/N$ is the time step, T is the time window (or sampling time), and N is the number of spectral components (or sampling number) up to the Nyquist frequency (Newland 1993).

Eq. (8) means that the time history of a moving point force given by Eq. (7) can be transformed to the frequency domain as a series of stationary point forces. Fig. 3 shows the series of stationary point forces distributed on a multi-span beam for a time window T chosen to be equal to the traveling time $T_A = L/v$ (*i.e.*, $T = T_A$). The frequency-domain representations of a moving point force for other cases, *i.e.*, when $T < T_A$ and when $T > T_A$, can be obtained from the literature (Song *et al.* 2016).

Assuming that the nth stationary point force F_n is located on the kth span, as shown in Fig. 3, the location of F_n is $x = x_n = vnT/N$ (see Eq. (10)). The kth span is located in $L_{k-1} \le x \le L_k$, where L_k is defined by Eq. (1). Thus, the span number k where F_n is located can be determined to satisfy the following condition

$$L_{k-1} \le \frac{vnT}{N} < L_k \tag{11}$$

If all spans of a multi-span beam have an equal length l, the span number k where F_n is located can be determined from Eq. (11) as follows

$$k = \left(\text{Integer part of } \frac{vnT}{Nl} \right) + 1 \; (n = 0,\ 1,\ 2,\ \ldots,\ N-1) \tag{12}$$

4.2 General procedures of spectral element vibration analysis

Once the moving point force is transformed to the frequency domain, the vibration analysis is conducted based on the superposition principle as follows:

(1) In the first step, the frequency-domain vibration responses $W^{(n)}(x,\omega)$ and $\Theta^{(n)}(x,\omega)$ of the multi-span beam due to stationary point force F_n are obtained using SEM.

(2) In the second step, once the frequency-domain vibration responses are obtained for all stationary point

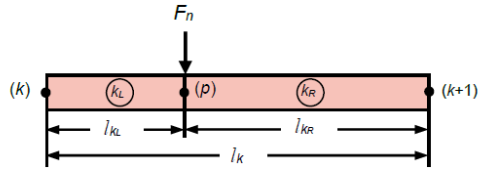

Fig. 6 Two-element model of the kth span subjected to a stationary point force F_n

forces, the total frequency-domain vibration responses are obtained using the superposition principle as follows

$$W(x,\omega)=\sum_{n=0}^{N-1}W^{(n)}(x,\omega),\quad \Theta(x,\omega)=\sum_{n=0}^{N-1}\Theta^{(n)}(x,\omega) \tag{13}$$

(3) In the last step, the time-domain vibration responses are obtained from Eq. (13) using the inverse fast Fourier transform (IFFT) algorithm (Newland 1993) as follows

$$w(x,t)=IFFT\,[W(x,\omega)],\quad \theta(x,t)=IFFT\,[\Theta(x,\omega)] \tag{14}$$

Based on the general procedure of spectral element vibration analysis, it suffices to focus the discussion on the first step where the frequency-domain vibration responses are obtained for stationary point force F_n (n = 0, 1, 2, …, N–1). In the following, the subscripts (n) are omitted for the brevity.

4.3 Dynamic responses to a stationary point force F_n

4.3.1 Assembly of spectral element equations

We assume that stationary point force F_n is located on the kth span of a multi-span beam as shown in Fig. 4. A benefit of SEM is that a uniform beam can be represented by a single spectral element, regardless of its length and with guaranteed exactness of the solutions. Thus, all spans except for the kth span can be represented by spectral element equations as follows

$$\boldsymbol{S}_m(\omega)\boldsymbol{d}_m=\boldsymbol{f}_m(\omega)\ (m=1,2,3,\ldots,k\text{–}1,k\text{+}1,\ldots,s) \tag{15}$$

where $\boldsymbol{S}_m(\omega)$ is the spectral element matrix for the mth span

$$\boldsymbol{S}_m(\omega)=\boldsymbol{S}(\omega,l=l_m) \tag{16}$$

$\boldsymbol{S}(\omega,l)$ is provided in Appendix A. As shown in Fig. 5, $\boldsymbol{d}_m$ is the nodal DOFs vector, and $\boldsymbol{f}_m$ is the nodal forces vector

$$\begin{aligned}\boldsymbol{d}_m&=\{W_m\ \ \Theta_m\ \ W_{m+1}\ \ \Theta_{m+1}\}^{\mathrm{T}}\\ \boldsymbol{f}_m&=\{Q_m\ \ M_m\ \ Q_{m+1}\ \ M_{m+1}\}^{\mathrm{T}}\end{aligned} \tag{17}$$

The kth span is subjected to F_n and can be represented by a two-element model, as shown in Fig. 6. The kth span is divided into two elements such that F_n is located at the joint node p where the left element k_L and the right element k_R are connected. The length of the left element is denoted by l_{k_L}, and the length of the right element is l_{k_R}. The spectral element equations for the left and right elements are as follows

$$\begin{aligned}\boldsymbol{S}_{k_L}(\omega)\boldsymbol{d}_{k_L}&=\boldsymbol{f}_{k_L}(\omega)\\ \boldsymbol{S}_{k_R}(\omega)\boldsymbol{d}_{k_R}&=\boldsymbol{f}_{k_R}(\omega)\end{aligned} \tag{18}$$

where

$$\boldsymbol{S}_{k_L}(\omega)=\boldsymbol{S}(\omega,l=l_{k_L}),\quad \boldsymbol{S}_{k_R}(\omega)=\boldsymbol{S}(\omega,l=l_{k_R}) \tag{19}$$

and

$$\begin{aligned}\boldsymbol{d}_{k_L}&=\{W_k\ \ \Theta_k\ \ W_p\ \ \Theta_p\}^{\mathrm{T}}\\ \boldsymbol{d}_{k_R}&=\{W_p\ \ \Theta_p\ \ W_{k+1}\ \ \Theta_{k+1}\}^{\mathrm{T}}\\ \boldsymbol{f}_{k_L}&=\{Q_k\ \ M_k\ \ -\tfrac{1}{2}F_n\ \ 0\}^{\mathrm{T}}\\ \boldsymbol{f}_{k_R}&=\{-\tfrac{1}{2}F_n\ \ 0\ \ Q_{k+1}\ \ M_{k+1}\}^{\mathrm{T}}\end{aligned} \tag{20}$$

A total of s+1 spectral element equations based on Eqs. (15) and (18) can be assembled using the technique commonly used in the standard finite element method to obtain an assembled global system equation in the following form

$$\boldsymbol{S}_g(\omega)\boldsymbol{d}_g=\boldsymbol{f}_g(\omega) \tag{21}$$

where $\boldsymbol{S}_g(\omega)$ is the global dynamic stiffness matrix, $\boldsymbol{d}_g$ is the global nodal DOFs vector, and $\boldsymbol{f}_g$ is the nodal forces vector

$$\boldsymbol{d}_g=\begin{Bmatrix}W_1\\ \Theta_1\\ W_2\\ \Theta_2\\ \vdots\\ W_k\\ \Theta_k\\ W_p\\ \Theta_p\\ W_{k+1}\\ \Theta_{k+1}\\ \vdots\\ W_s\\ \Theta_s\\ W_{s+1}\\ \Theta_{s+1}\end{Bmatrix},\quad \boldsymbol{f}_g=\begin{Bmatrix}Q_1\\ M_1\\ Q_2\\ M_2\\ \vdots\\ Q_k\\ M_k\\ -F_n\\ 0\\ Q_{k+1}\\ M_{k+1}\\ \vdots\\ Q_s\\ M_s\\ Q_{s+1}\\ M_{s+1}\end{Bmatrix} \tag{22}$$

where Q_r and M_r (r = 1, 2, 3, …, s+1) represent the reaction forces and moments at the interim supports and boundaries at x = 0 and L.

4.3.2 Imposition of boundary conditions

The components of Eq. (22) can be rearranged to define new vectors as follows

$$\hat{\boldsymbol{d}}_g=\begin{Bmatrix}\boldsymbol{d}_L\\ \boldsymbol{d}_R\\ \boldsymbol{d}_p\end{Bmatrix}=\begin{Bmatrix}\boldsymbol{d}_B\\ \boldsymbol{d}_p\end{Bmatrix},\quad \hat{\boldsymbol{f}}_g=\begin{Bmatrix}\boldsymbol{f}_L\\ \boldsymbol{f}_R\\ \boldsymbol{f}_p\end{Bmatrix}=\begin{Bmatrix}\boldsymbol{f}_B\\ \boldsymbol{f}_p\end{Bmatrix} \tag{23}$$

where

$$\begin{aligned}\boldsymbol{d}_L&=\{W_1\ \Theta_1\ W_2\ \Theta_2\cdots W_k\ \Theta_k\}^{\mathrm{T}}\\ \boldsymbol{d}_R&=\{W_{k+1}\Theta_{k+1}\cdots W_s\ \Theta_s\ W_{s+1}\ \Theta_{s+1}\}^{\mathrm{T}}\\ \boldsymbol{d}_p&=\{W_p\ \Theta_p\}^{\mathrm{T}}\\ \boldsymbol{f}_L&=\{Q_1\,M_1\,Q_2\,M_2\cdots Q_k\,M_k\}^{\mathrm{T}}\\ \boldsymbol{f}_R&=\{Q_{k+1}\,M_{k+1}\cdots Q_s\ M_s\,Q_{s+1}\,M_{s+1}\}^{\mathrm{T}}\\ \boldsymbol{f}_p&=\{-F_n\ \ 0\}^{\mathrm{T}}\end{aligned} \tag{24}$$

Table 1 Boundary matrices $\boldsymbol{B}_i^d$ and $\boldsymbol{B}_i^f$ for various boundary conditions

Boundary conditions	$\boldsymbol{B}_i^d$	$\boldsymbol{B}_i^f$
Simply supported	$\begin{bmatrix}\boldsymbol{0}_{2\times a} & \boldsymbol{L} & \boldsymbol{0}_{2\times b}\end{bmatrix}$	$\begin{bmatrix}\boldsymbol{0}_{2\times c} & \boldsymbol{U} & \boldsymbol{0}_{2\times d}\end{bmatrix}$
Clamped	$\begin{bmatrix}\boldsymbol{0}_{2\times e}\end{bmatrix}$	$\begin{bmatrix}\boldsymbol{0}_{2\times c} & \boldsymbol{I}_2 & \boldsymbol{0}_{2\times d}\end{bmatrix}$
Free	$\begin{bmatrix}\boldsymbol{0}_{2\times a} & \boldsymbol{I}_2 & \boldsymbol{0}_{2\times b}\end{bmatrix}$	$\begin{bmatrix}\boldsymbol{0}_{2\times e}\end{bmatrix}$

Note: (1) $a = s_1+2f_1$, $b = s_1+2c_1$, $c = s_2+2f_2$, $d = s_2+2c_2$, and e = length of vector $\bar{\boldsymbol{d}}_B$, where s_1, f_1, and c_1 are the numbers of simply supported, free, and clamped nodes before the ith node, and s_2, f_2, and c_2 are the numbers after the ith node, respectively, (2) $\boldsymbol{L} = \{0\ 1\}^{\mathrm{T}}$, $\boldsymbol{U} = \{1\ 0\}^{\mathrm{T}}$

and

$$\boldsymbol{d}_B = \begin{Bmatrix}\boldsymbol{d}_L \\ \boldsymbol{d}_R\end{Bmatrix}, \quad \boldsymbol{f}_p = \begin{Bmatrix}\boldsymbol{f}_L \\ \boldsymbol{f}_R\end{Bmatrix} \tag{25}$$

The global nodal DOFs vector $\boldsymbol{d}_g$ and the global nodal forces vector $\boldsymbol{f}_g$ can be related to newly-defined vectors $\hat{\boldsymbol{d}}_g$ and $\hat{\boldsymbol{f}}_g$ as follows

$$\boldsymbol{d}_g = \boldsymbol{R}\hat{\boldsymbol{d}}_g, \quad \boldsymbol{f}_g = \boldsymbol{R}\hat{\boldsymbol{f}}_g \tag{26}$$

where $\boldsymbol{R}$ is the transformation matrix defined by

$$\boldsymbol{R} = \begin{bmatrix}\boldsymbol{I}_{2k} & \boldsymbol{0} & \boldsymbol{0} \\ \boldsymbol{0} & \boldsymbol{0} & \boldsymbol{I}_2 \\ \boldsymbol{0} & \boldsymbol{I}_{2(s-k+1)} & \boldsymbol{0}\end{bmatrix} \tag{27}$$

where $\boldsymbol{0}$ denotes a zero matrix, and $\boldsymbol{I}$ denotes an identity matrix, with subscripts indicating the dimensions of identity matrices. The transformation matrix $\boldsymbol{R}$ satisfies

$$\boldsymbol{R}^{\mathrm{T}}\boldsymbol{R} = \boldsymbol{I} \tag{28}$$

By imposing geometric boundary conditions on the interim supports and two boundaries at $x = 0$ and $x = L$, the original nodal DOFs vector $\boldsymbol{d}_B$ can be related to the reduced nodal DOFs vector $\bar{\boldsymbol{d}}_B$ as follows

$$\boldsymbol{d}_B = \boldsymbol{B}^d\bar{\boldsymbol{d}}_B \tag{29}$$

Similarly, by imposing natural boundary conditions, the original nodal forces vector $\boldsymbol{f}_B$ can be related to the reduced nodal forces vector $\bar{\boldsymbol{f}}_B$ as follows

$$\boldsymbol{f}_B = \boldsymbol{B}^f\bar{\boldsymbol{f}}_B \tag{30}$$

The matrices $\boldsymbol{B}^d$ and $\boldsymbol{B}^f$ in Eqs. (29) and (30) are defined by

$$\boldsymbol{B}^d = \begin{bmatrix}\boldsymbol{B}_1^d \\ \boldsymbol{B}_2^d \\ \vdots \\ \boldsymbol{B}_i^d \\ \vdots \\ \boldsymbol{B}_s^d \\ \boldsymbol{B}_{s+1}^d\end{bmatrix}, \quad \boldsymbol{B}^f = \begin{bmatrix}\boldsymbol{B}_1^f \\ \boldsymbol{B}_2^f \\ \vdots \\ \boldsymbol{B}_i^f \\ \vdots \\ \boldsymbol{B}_s^f \\ \boldsymbol{B}_{s+1}^f\end{bmatrix} \tag{31}$$

where $\boldsymbol{B}_i^d$ and $\boldsymbol{B}_i^f$ are the boundary matrices for the ith node and are given in Table 1 for various boundary conditions. The matrices $\boldsymbol{B}^d$ and $\boldsymbol{B}^f$ satisfy the following relations (Song *et al*. 2016)

$$(\boldsymbol{B}^d)^{\mathrm{T}}\boldsymbol{B}^f = \boldsymbol{0}, \quad (\boldsymbol{B}^f)^{\mathrm{T}}\boldsymbol{B}^d = \boldsymbol{0} \tag{32}$$

By using Eqs. (29) and (30), Eq. (23) can be written in the following forms

$$\hat{\boldsymbol{d}}_g = \bar{\boldsymbol{B}}^d\bar{\boldsymbol{d}}_g, \quad \hat{\boldsymbol{f}}_g = \bar{\boldsymbol{B}}^f\bar{\boldsymbol{f}}_g \tag{33}$$

where

$$\bar{\boldsymbol{d}}_g = \begin{Bmatrix}\bar{\boldsymbol{d}}_B \\ \boldsymbol{d}_p\end{Bmatrix}, \quad \bar{\boldsymbol{f}}_g = \begin{Bmatrix}\bar{\boldsymbol{f}}_B \\ \boldsymbol{f}_p\end{Bmatrix} \tag{34}$$

and

$$\bar{\boldsymbol{B}}^d = \begin{bmatrix}\boldsymbol{B}^d & \boldsymbol{0} \\ \boldsymbol{0} & \boldsymbol{I}_2\end{bmatrix}, \quad \bar{\boldsymbol{B}}^f = \begin{bmatrix}\boldsymbol{B}^f & \boldsymbol{0} \\ \boldsymbol{0} & \boldsymbol{I}_2\end{bmatrix} \tag{35}$$

Substituting Eq. (33) into Eq. (26) gives

$$\boldsymbol{d}_g = \boldsymbol{R}\bar{\boldsymbol{B}}^d\bar{\boldsymbol{d}}_g, \quad \boldsymbol{f}_g = \boldsymbol{R}\bar{\boldsymbol{B}}^f\bar{\boldsymbol{f}}_g \tag{36}$$

By substituting Eq. (36) into Eq. (21), multiplying both sides of the result by $(\bar{\boldsymbol{B}}^d)^{\mathrm{T}}\boldsymbol{R}^{\mathrm{T}}$, and using Eqs. (28) and (36), the original assembled global system equation, Eq. (21), can be reduced to the following form

$$\bar{\boldsymbol{S}}_g\bar{\boldsymbol{d}}_g = \tilde{\boldsymbol{f}}_g \tag{37}$$

where

$$\bar{\boldsymbol{S}}_g = (\bar{\boldsymbol{B}}^d)^{\mathrm{T}}\boldsymbol{R}^{\mathrm{T}}\boldsymbol{S}_g\boldsymbol{R}\bar{\boldsymbol{B}}^d \tag{38}$$

and

$$\tilde{\boldsymbol{f}}_g = \begin{Bmatrix}\boldsymbol{0} \\ \boldsymbol{f}_p\end{Bmatrix} \tag{39}$$

4.3.3 Computation of vibration responses

The global nodal DOF vector $\boldsymbol{d}_g$ can be obtained by first solving Eq. (37) for $\bar{\boldsymbol{d}}_g$ and then substituting the result into Eq. (36)

$$\boldsymbol{d}_g = \boldsymbol{R}\bar{\boldsymbol{B}}^d(\bar{\boldsymbol{S}}_g)^{-1}\tilde{\boldsymbol{f}}_g \tag{40}$$

To compute the frequency-domain vibration responses in the mth span, we consider two cases where (a) m = 1, 2, 3, …, k–1, k+1, …, s and (b) $m = k$.

(a) m = 1, 2, 3, …, k-1, k+1,…, s

The nodal DOFs vector $\boldsymbol{d}_m$ defined by Eq. (17) for the mth span can be related to the global nodal DOFs vector $\boldsymbol{d}_g$ as follows

$$\boldsymbol{d}_m = \boldsymbol{T}_m\boldsymbol{d}_g \tag{41}$$

where

$$\boldsymbol{T}_m = \begin{bmatrix}\boldsymbol{0}_{4\times 2q} & \boldsymbol{I}_4 & \boldsymbol{0}_{4\times 2(s-q)}\end{bmatrix} \tag{42}$$

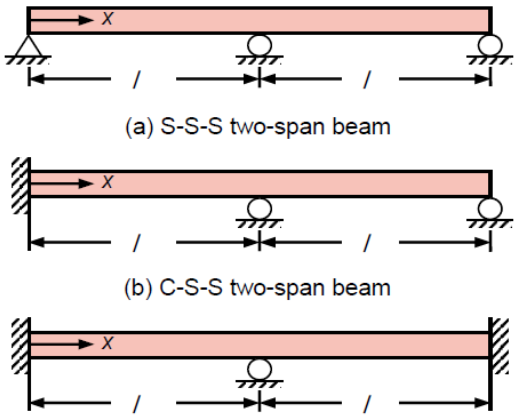

Fig. 7 Three examples of two-span beams subjected to a moving point force P

where $q = m–1$ if $m < k$ and $q = m$ if $m > k$. Once $\boldsymbol{d}_m$ is computed from Eq. (41), the frequency-domain vibration responses in the mth span can be computed from

$$W_m(x,\omega) = \boldsymbol{N}_w(x,\omega;l=l_m)\boldsymbol{d}_m \quad (L_{m-1} \le x \le L_m) \qquad (43)$$
$$\Theta_m(x,\omega) = \boldsymbol{N}_\theta(x,\omega;l=l_m)\boldsymbol{d}_m$$

where $\boldsymbol{N}_w(x,\omega;l)$ and $\boldsymbol{N}_\theta(x,\omega;l)$ are one-by-four dynamic shape functions defined in the previous study (Lee 2009).

(b) $m = k$

The kth span is represented by two elements, k_L and k_R, as shown in Fig. 6. The nodal DOFs for these two elements are represented by $\boldsymbol{d}_{k_L}$ and $\boldsymbol{d}_{k_R}$, which are defined by Eq. (20). The nodal DOFs vectors $\boldsymbol{d}_{k_L}$ and $\boldsymbol{d}_{k_R}$ can be related to the global nodal DOFs vector $\boldsymbol{d}_g$ as follows

$$\boldsymbol{d}_{k_L} = \boldsymbol{T}_{k_L}\boldsymbol{d}_g$$
$$\boldsymbol{d}_{k_R} = \boldsymbol{T}_{k_R}\boldsymbol{d}_g \qquad (44)$$

where

$$\boldsymbol{T}_{k_L} = \left[\boldsymbol{0}_{4\times 2(k-1)} \quad \boldsymbol{I}_4 \quad \boldsymbol{0}_{4\times 2(s-k+1)}\right]$$
$$\boldsymbol{T}_{k_R} = \left[\boldsymbol{0}_{4\times 2k} \quad \boldsymbol{I}_4 \quad \boldsymbol{0}_{4\times 2(s-k)}\right] \qquad (45)$$

The frequency-domain vibration responses in the kth span can be computed from

$$W_k(x,\omega) = \begin{cases} \boldsymbol{N}_w(x,\omega;l=l_{k_L})\boldsymbol{d}_{k_L} & (L_{k-1} \le x \le L_{k-1}+l_{k_L}) \\ \boldsymbol{N}_w(x,\omega;l=l_{k_R})\boldsymbol{d}_{k_R} & (L_{k-1}+l_{k_L} \le x \le L_k) \end{cases}$$
$$\Theta_k(x,\omega) = \begin{cases} \boldsymbol{N}_\theta(x,\omega;l=l_{k_L})\boldsymbol{d}_{k_L} & (L_{k-1} \le x \le L_{k-1}+l_{k_L}) \\ \boldsymbol{N}_\theta(x,\omega;l=l_{k_R})\boldsymbol{d}_{k_R} & (L_{k-1}+l_{k_L} \le x \le L_k) \end{cases} \qquad (46)$$

Based on Eqs. (43) and (46), the frequency-domain vibration responses at an arbitrary position x are

$$W^{(n)}(x,\omega) = \sum_{m=1}^{s} W_m(x,\omega)H_m(x)$$
$$\Theta^{(n)}(x,\omega) = \sum_{m=1}^{s} \Theta_m(x,\omega)H_m(x) \qquad (47)$$

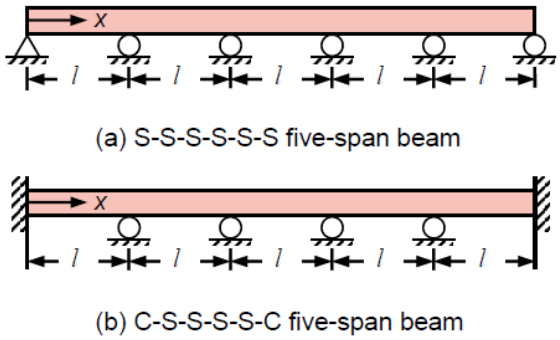

Fig. 8 Two examples of five-span beams subjected to a moving point force P

where

$$H_m(x) = h(x-L_{m-1}) - h(x-L_m) \qquad (48)$$

where $h(x)$ is the Heaviside step function (Kreyszig 1972).

$$h(x) = \begin{cases} 0 & (x<0) \\ 1 & (x \ge 0) \end{cases} \qquad (49)$$

As mentioned in Section 4.2, the frequency-domain vibration analysis is repeated N times to obtain $W^{(n)}(x,\omega)$ and $\Theta^{(n)}(x,\omega)$ for all stationary point forces F_n, where $n = 0$, 1, 2, …, N–1. Next, the total frequency-domain vibration responses are obtained from Eq. (13), based on the superposition principle. Finally, the time-domain vibration responses can be obtained from these total frequency-domain vibration responses by using the IFFT algorithm (Newland 1993).

5. Numerical results and discussion

For numerical studies, we consider three two-span beams shown in Fig. 7: a simple-simple-simple (S-S-S) supported beam, a clamped-simple-simple (C-S-S) supported beam, and a clamped-simple-clamped (C-S-C) supported beam. We also consider two five-span beams shown in Fig. 8: a simple-simple-simple-simple-simple-simple (S-S-S-S-S-S) support-ed beam and a clamped-simple-simple-simple-simple-clamped (C-S-S-S-S-C) supported beam. The geometric and material properties of each span of the example multi-span beams are as follows: length l = 4.352 m, cross-sectional area $A = 1.31\times10^{-3}$ m^2, the area moment of inertia $I = 5.71\times10^{-7}$ m^4, Young's modulus $E = 2.02\times10^{11}$ N/m^2, shear modulus $G = 7.7\times10^{10}$ N/m^2, mass density ρ = 15,267 kg/m^3, and shear correction factor κ = 0.7. We assume that all example multi-span beams are subjected to a moving point force with constant magnitude P = 1 kN and constant speed v = 20, 50, or 80 m/s.

To evaluate the proposed method, the natural frequencies and vibration responses of the S-S-S two-span beam and S-S-S-S-S-S five-span beam obtained by SEM are first compared with results obtained by standard FEM. All FEM results were obtained using the finite element mass and stiffness matrices for a Timoshenko beam model

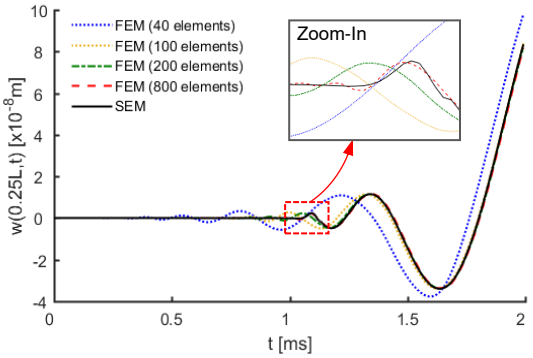

Fig. 9 Comparison of the short-term early-phase vibration responses of an S-S-S two-span beam obtained by the proposed SEM and by FEM (Wu *et al*. 2000) for v=20 m/s

Table 2 Natural frequencies (Hz) of an S-S-S two-span beam obtained by the proposed SEM and by FEM (Petyt 2010)

Mode number	FEM				SEM
	n=20	n=50	n=100	n=300	n=2
1	6.295	6.295	6.295	6.295	6.295
2	9.826	9.826	9.826	9.826	9.826
3	25.14	25.14	25.14	25.14	25.14
4	31.78	31.77	31.77	31.77	31.77
5	56.46	56.42	56.41	56.41	56.41
10	172.0	170.9	170.8	170.8	170.8
15	402.9	391.1	390.2	390.0	390.0

Note: n = total number of finite elements used in the analysis

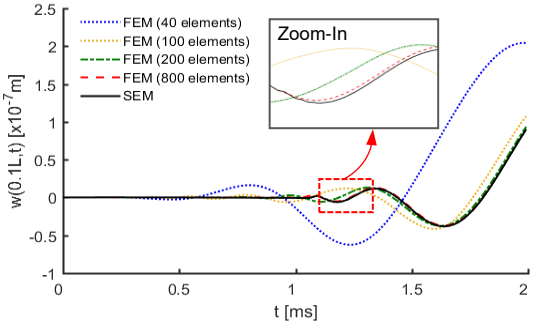

Fig. 10 Comparison of the short-term early-phase vibration responses of an S-S-S-S-S-S five span beam obtained by the proposed SEM and by FEM (Wu *et al*. 2000) for v=20 m/s

introduced by Petyt (2010). Tables 2 and 3 compare the natural frequencies of the S-S-S two-span beam and S-S-S-S-S-S five-span beam obtained by SEM and FEM. For the FEM results, the total number of equal-length finite elements used in the analysis is increased until the first four converges. However, the SEM results are obtained using only two finite elements for the S-S-S two-span beam and only five finite elements for the S-S-S-S-S-S five-span beam. That is, only a single finite element is used for each span of the multi-span beam examples. The tables show that the FEM results converge to the SEM results as the total

Table 3 Natural frequencies (Hz) of an S-S-S-S-S-S five-span beam obtained by the proposed SEM and by FEM (Petyt 2010)

Mode number	FEM				SEM
	n=20	n=50	n=100	n=200	n=5
1	6.297	6.295	6.295	6.295	6.295
2	6.985	6.983	6.983	6.983	6.983
3	8.733	8.728	8.728	8.728	8.728
4	11.00	10.99	10.99	10.99	10.99
5	13.20	13.19	13.19	13.19	13.19
10	37.77	37.45	37.43	37.43	37.43
15	75.90	74.17	74.08	74.07	74.07

Note: n = total number of finite elements used in the analysis

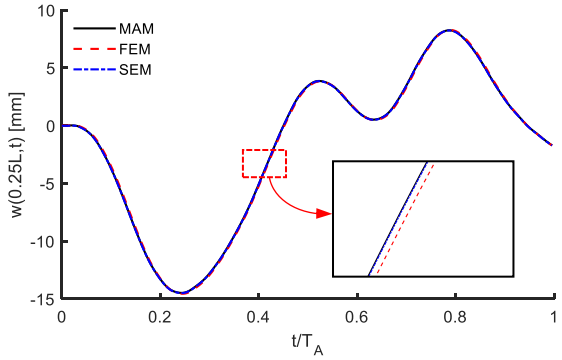

Fig. 11 Comparison of the long-term vibration responses of the S-S-S two-span Timoshenko beam obtained by the modal analysis method (MAM) (Wang 1997), FEM (Wu *et al*. 2000) and the present SEM for v=20 m/s

number of finite element increases.

Fig. 9 compares the short-term transverse vibration responses in the early phase at $x = 0.25L$ of the S-S-S two-span obtained by SEM and FEM, where $L = 2l$. Similarly, Fig. 10 compares the short-term early-phase responses at $x = 0.1L$ for the S-S-S-S-S-S five-span beam, where $L = 5l$. The FEM-based vibration responses were obtained using the finite element analysis technique introduced by Wu *et al.* (2000) for moving load problems. For the results in Figs. 9 and 10, it is assumed that the speed of the moving point force is v = 20 m/s. It is clear from the figures that the short-term early-phase responses obtained by FEM converge to the results by the SEM as the total number of finite elements increases. The computation times (CPU times on a desktop PC with an Intel core i7-3770 CPU) required to obtain the short-term early-phase responses of the S-S-S two-span are about 19 seconds for the present SEM and 74 seconds for the FEM using 800 elements.

Exact analytical solutions are very rare for multi-span beams subjected to moving loads. Wang (1997) presented a modal analysis method (MAM) to obtain analytical solutions for the multi-span Timoshenko beams subjected to a moving force. The MAM by Wang (1997) was applied to the S-S-S two-span Timoshenko beam to obtain long-term transverse vibration responses for v = 20 m/s. In Fig. 11, the present

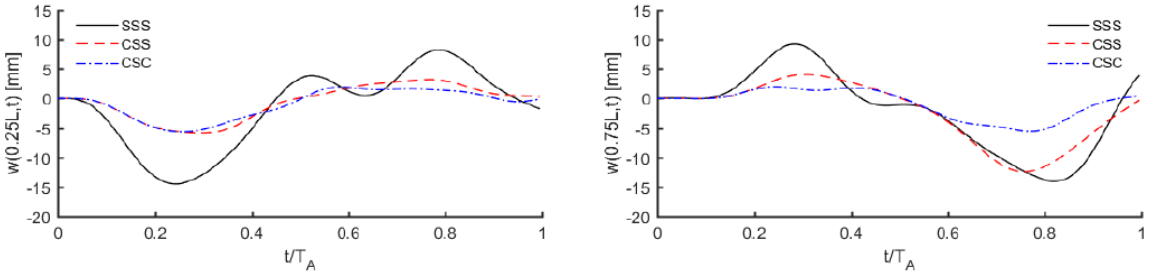

Fig. 12 Effects of boundary conditions on the long-term vibration responses at $x=0.25L$ and $0.75L$ of a two-span beam ($L=2l$) for $v=20$ m/s

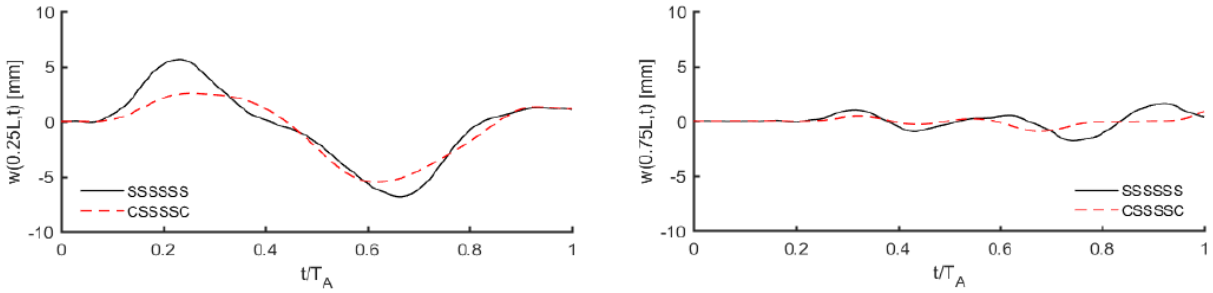

Fig. 13 Effects of boundary conditions on the long-term vibration responses at $x=0.25L$ and $0.75L$ of a five-span beam ($L=5l$) for $v=20$ m/s

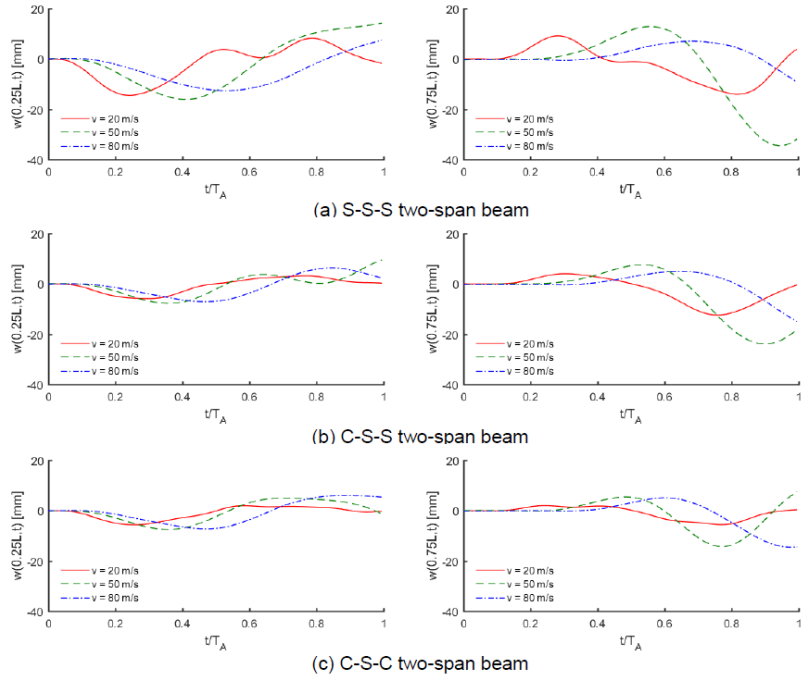

Fig. 14 Effects of moving speed (v) on the long-term vibration responses at $x=0.25L$ and $0.75L$ of the S-S-S, C-S-S, and C-S-C two-span beams ($L=2l$)

SEM results are compared with the analytical solutions by MAM and the FEM results obtained using 800 elements. In Fig. 11, $T_A = L/v$ denotes the time required for the moving point force to travel from the left end ($x = 0$) to the right end ($x = L$) of the beam. Fig. 11 shows that the SEM results are almost identical to the analytical solutions by MAM and the FEM results. Overall, the results show that the proposed SEM is very accurate and efficient.

The effects of the boundary conditions and the moving speed (v) of a point force on the transverse vibration responses are numerically investigated by using the present SEM for three two-span beam examples (see Fig. 7) and two boundary conditions at $x = 0$ and L, where $L = 2l$ for the two-span beams and $L = 5l$ for the five-span beams.

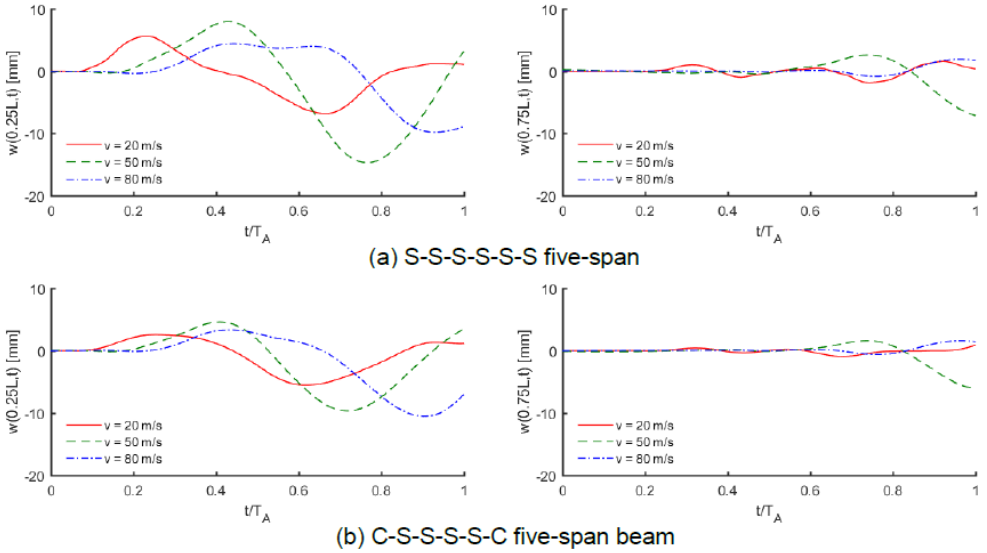

Fig. 15 Effects of moving speed (v) on the long-term vibration responses at $x=0.25L$ and $0.75L$ of the S-S-S, C-S-S, and C-S-C two-span beams ($L=2l$)

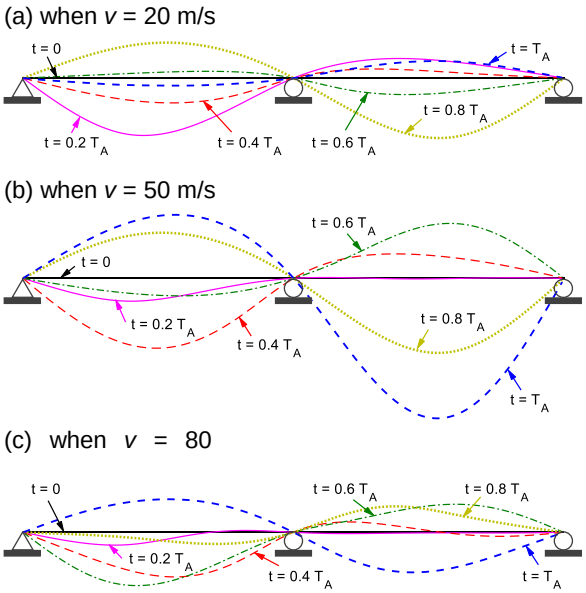

Fig. 16 Time-dependent deformed shapes of the S-S-S two-span beam subjected to a moving point force for $v=20$, 50, and 80 m/s

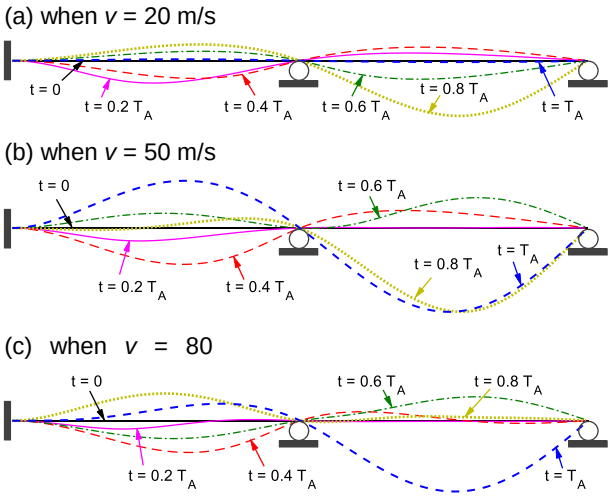

Fig. 17 Time-dependent deformed shapes of the C-S-S two-span beam subjected to a moving point force for $v=20$, 50, and 80 m/s

Fig. 12 compares the long-term transverse vibration responses at $x = 0.25L$ and $0.75L$ for the two-span beams using $v = 20$ m/s. Similarly, Fig. 13 compares the responses at $x = 0.25L$ and $0.75L$ of for the five-span beams using $v = 20$ m/s. The figures show that the vibration responses are strongly dependent on the boundary conditions and the maximum magnitudes of the transverse vibration responses become smaller as more boundaries are clamped, which is physically natural.

Figs. 14 and 15 show the effects of the speed (v) of the moving point force on the long-term transverse vibration responses are strongly dependent on the speed of the moving point force and the vibration responses at $v = 50$ m/s seem larger than those at $v = 20$ and 80 m/s, especially when all boundaries and internal supports are simply

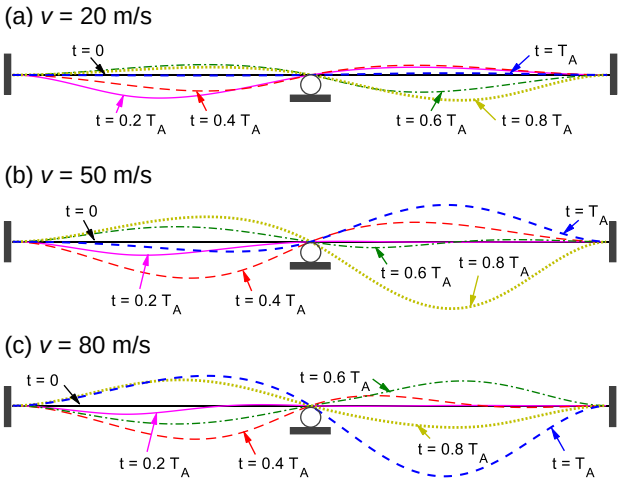

Fig. 18 Time-dependent deformed shapes of the C-S-C two-span beam subjected to a moving point force for $v=20$, 50, and 80 m/s

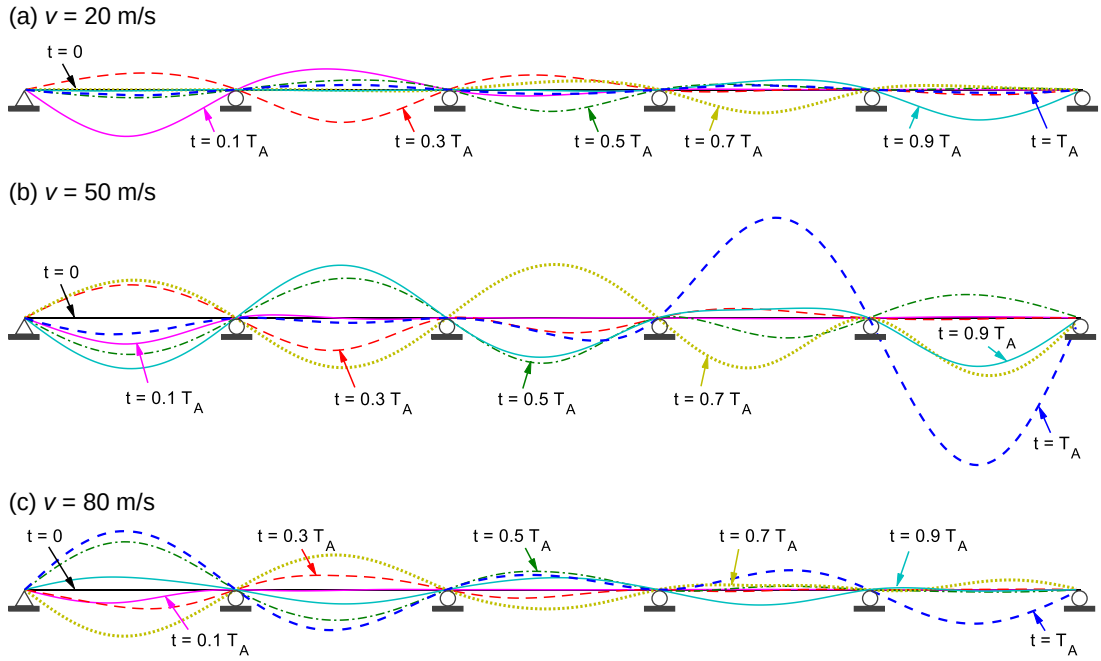

Fig. 19 Time-dependent deformed shapes of the S-S-S-S-S-S five-span beam subjected to a moving point force for v=20, 50, and 80 m/s

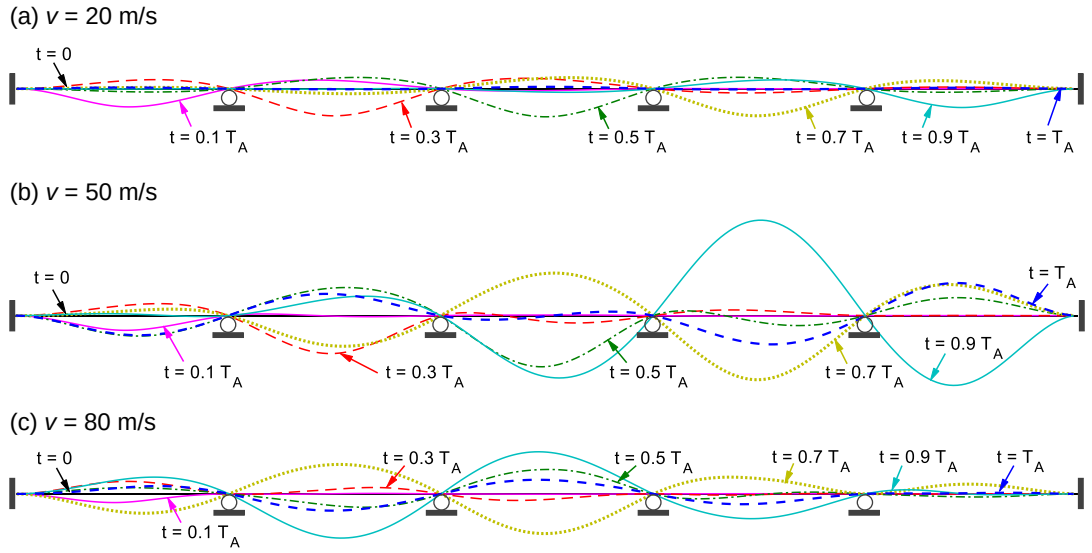

Fig. 20 Time-dependent deformed shapes of the C-S-S-S-S-C five-span beam subjected to a moving point force for v=20, 50, and 80 m/s

supported. This occurs because v= 50 m/s is closest to the critical moving speed (v_{cr} = 54.79 m/s) where resonance vibrations can occur for a single-span simply supported beam of length l (Frýba 1999).

Fig. 16 compares the deformed shapes of the S-S-S two-span beam at t = 0, 0.2T_A, 0.4T_A, 0.6T_A, 0.8T_A, and T_A for speeds v = 20, 50, and 80 m/s. Figs. 17 and 18 compares the deformed shapes for the C-S-S and C-S-C two-span beams, respectively. T_A = 2l/v denotes the time required for the moving point force to travel from the left end (x = 0) to the right end (x = 2l). The figures show that the deformed shapes strongly dependent on the speed of the moving point force and the boundary conditions. As observed from Fig. 14, the magnitudes of the deformed shapes seem to be largest when the speed is near the critical speed, especially for the case of the S-S-S two-span beam. The S-S-S two-span beam is geometrically symmetric with respect to the mid-point (x = l). However, in contrast to the static problems, the deformed shapes are not symmetric when the moving point force passes two points that are at equidistant from both ends of the beam (*i.e.*, at t = 0 and T_A, at 0.2T_A and 0.8T_A, or at 0.4T_A and 0.6T_A). This is due to the convolution of the casual effect of the moving point force.

Lastly, Fig. 19 compares the deformed shapes for the S-S-S-S-S-S five-span beam at t = 0, 0.1T_A, 0.3T_A, 0.5T_A, 0.7T_A, 0.9T_A, and T_A for different speeds of the moving

point force. Fig. 20 compares the deformed shapes for the C-S-S-S-S-C five-span beams. $T_A = 5l/v$ denotes the time required for the moving point force to travel from the left end ($x = 0$) to the right end ($x = 5l$) of the beams. The results in these cases are very similar to those observed from Figs. 16, 17 and 18.

6. Conclusions

This study has presented a two-element model-based frequency domain spectral element analysis method for the vibrations of a multi-span beam subjected to a moving point force as an extension of the previous work for a single-span beam. A time-domain moving point force is transformed into the frequency domain as a series of stationary point forces acting on a multi-span beam simultaneously. The vibration responses in both the frequency domain and time domain are obtained by superposing all individual vibration responses due to each stationary point force. To obtain the individual vibration responses to a specific stationary point force, the span where the stationary point force is located is represented by a two-element model, while all other spans are represented by one-element models. The followings were investigated through numerical studies:

(1) The high accuracy and computational efficiency of the proposed method was verified by comparing it with exact ITM solutions and FEM.

(2) The vibration responses are strongly dependent on the boundary conditions and the speed of the moving point force.

(3) In general, the vibration responses are large when the speed of the moving point force is near the critical speed for a simply supported single-span beam.

(4) In contrast to static problems, the deformed shapes are not symmetric with respect to the mid-point of a multi-span beam at the times when a moving point force passes two points that are at equidistant from both ends of the beam due to the convolution of the casual effect.

Acknowledgments

This work was supported by the Inha University research grant.

References

Ariaei, A., Ziaei-Rad, S. and Ghayour, M. (2011), "Transverse vibration of a multiple-Timoshenko beam system with intermediate elastic connections due to a moving load", *Arch. Appl. Mech.*, **81**(3), 263-281.

Ariaei, A., Ziaei-Rad, S. and Malekzdeh, M. (2013), "Dynamic response of a multi-span Timoshenko beam with internal and external flexible constraints subject to a moving mass", *Arch. Appl. Mech.*, **83**(9), 1257-1272.

Asnachinda, P., Pinkaew, T. and Laman, J.A. (2008), "Multiple vehicle axle load identification from continuous bridge bending moment response", *Eng. Struct.*, **30**(10), 2800-2817.

Azizi, N., Saadatpour, M.M. and Mahzoon, M. (2012), "Using spectral element method for analyzing continuous beams and bridges subjected to a moving load", *Appl. Math. Model.*, **36**(8), 3580-3592.

Cai, C.W., Cheung, Y.K. and Chan, H.C. (1988), "Dynamic response of infinite continuous beams subjected to a moving force-an exact method", *J. Sound Vibr.*, **123**(3), 461-472.

Chan, T.H.T. and Ashebo, D.B. (2006), "Theoretical study of moving force identification on continuous bridges", *J. Sound Vibr.*, **295**(3), 870-883.

Cheung, Y.K., Au, F.T.K., Zheng, D.Y. and Cheng, Y.S. (1999), "Vibration of multi-span non-uniform bridges under moving vehicles and trains by using modified beam vibration functions", *J. Sound Vibr.*, **228**(3), 611-628.

De Salvo, V., Muscolino, G. and Palmeri, A. (2010), "A substructure approach tailored to the dynamic analysis of multi-span continuous beams under moving loads", *J. Sound Vibr.*, **329**(15), 3101-3120.

Dmitriev, A.S. (1974), "Transverse vibrations of a three-span beam under a moving load", *Appl. Mech.*, **10**(11), 1263-1266.

Dmitriev, A.S. (1977), "Transverse vibrations of a two-span beam with elastic central support under the action of a moving point force", *Appl. Mech.*, **13**(11), 1160-1163.

Dmitriev, A.S. (1982), "Dynamics of continuous multispan beams under a moving force", *Appl. Mech.*, **18**(2), 179-186.

Dugush, Y.A. and Eisenberger, M. (2002), "Vibrations of non-uniform continuous beams under moving loads", *J. Sound Vibr.*, **254**(5), 911-926.

Frýba, L. (1999), *Vibration of Solids and Structures under Moving Loads*, Thomas Telford Publishing, London.

Henchi, K., Fafard, M., Dhatt, G. and Talbot, M. (1997), "Dynamic behaviour of multi-span beams under moving loads", *J. Sound Vibr.*, **199**(1), 33-50.

Hong, S.W. and Kim, J.W. (1999), "Modal analysis of multi-span Timoshenko beams connected or supported by resilient joints with damping", *J. Sound Vibr.*, **227**(4), 787-806.

Ichikawa, M., Miyakawa, Y. and Matuda, A. (2000), "Vibration analysis of the continuous beam subjected to a moving mass", *J. Sound Vibr.*, **230**(3), 493-506.

Jiang, R.J., Au, F.T.K. and Cheung, Y.K. (2004), "Identification of vehicles moving on continuous bridges with rough surface", *J. Sound Vibr.*, **274**(3), 1045-1063.

Johansson, C., Pacoste, C. and Karoumi, R. (2013), "Closed-form solution for the mode superposition analysis of the vibration in multi-span beam bridges caused by concentrated moving loads", *Comput. Struct.*, **119**, 85-94.

Kiani, K., Nikkhoo, A. and Mehri, B. (2010), "Assessing dynamic response of multispan viscoelastic thin beams under a moving mass via generalized moving least square method", *Acta Mech. Sin.*, **26**(5), 721-733.

Kim, T., Park, I. and Lee, U. (2017), "Forced vibration of a Timoshenko beam subjected to stationary and moving loads using the modal analysis method", *Shock Vibr.*, 3924921.

Krawczuk, M., Palacz, M. and Ostachowicz, W. (2003), "The dynamic analysis of a cracked Timoshenko beam by the spectral element method", *J. Sound Vibr.*, **264**(5), 1139-1153.

Kreyszig, E. (1972), *Advanced Engineering Mathematics*, John Wiley & Sons, New Jersey, U.S.A.

Kwon, H.C., Kim, M.C. and Lee, I.W. (1998), "Vibration control of bridges under moving loads", *Comput. Struct.*, **66**(4), 473-480.

Lee, H.P. (1994), "Dynamic response of a beam with intermediate point constraints subject to a moving load", *J. Sound Vibr.*, **171**(3), 361-368.

Lee, H.P. (1996), "Dynamic response of a beam on multiple supports with a moving mass", *Struct. Eng. Mech.*, **4**(3), 303-312.

Lee, U. (2009), *Spectral Element Method in Structural Dynamics*, John Wiley & Sons, Singapore.

Li, W.L. and Xu H. (2009), "An exact Fourier series method for the vibration analysis of multispan beam systems", *J. Comput. Nonlin. Dyn.*, **4**(2), 021001.
Lou, P. and Au, F.T.K. (2013), "Finite element formulae for internal forces of Bernoulli-Euler beams under moving vehicles", *J. Sound Vibr.*, **332**(6), 1533-1552.
Lou, P., Yu, Z.W. and Au, F.T.K. (2012), "Rail-bridge coupling element of unequal lengths for analysing train-track-bridge interaction systems", *Appl. Math. Model.*, **36**(4), 1395-1414.
Martinez-Castro, A.E., Museros, P. and Castillo-Linares, A. (2006), "Semi-analytic solution in the time domain for non-uniform multi-span Bernoulli-Euler beams traversed by moving loads", *J. Sound Vibr.*, **294**(1), 278-297.
Newland, D.E. (1993), *Random Vibrations: Spectral and Wavelet Analysis*, Longman, New York, U.S.A.
Petyt, M. (2010), *Introduction to Finite Element Vibration Analysis*, Cambridge University Press, New York, U.S.A.
Sarvestan, V., Mirdamadi, H.R., Ghayour, M. and Mokhtari, A. (2015), "Spectral finite element for vibration analysis of cracked viscoelastic Euler-Bernoulli beam subjected to moving load", *Acta Mech.*, **226**(12), 4259-4280.
Song, Y., Kim, T. and Lee, U. (2016), "Vibration of a beam subjected to a moving force: Frequency-domain spectral element modeling and analysis", *J. Mech. Sci.*, **113**, 162-174.
Szylko-Bigus, O. and Sniady, P. (2015), "Dynamic response of a Timoshenko beam to a continuous distributed moving load", *Struct. Eng. Mech.*, **54**(4), 771-792.
Tang, C.C. and Wang, Y.C. (2002), "Dynamic characteristics of elastic beams subjected to traffic loads", *Struct. Eng. Mech.*, **13**(2), 211-230.
Tehrani, M. and Eipakchi, H.R. (2012), "Response determination of a viscoelastic Timoshenko beam subjected to moving load using analytical and numerical methods", *Struct. Eng. Mech.*, **44**(1), 1-13.
Wang, J.F. and Lin, C.C. and Chen, B.L. (2003), "Vibration suppression for high-speed railway bridges using tuned mass dampers", *J. Sol. Struct.*, **40**(2), 465-491.
Wang, R.T. (1997), "Vibration of multi-span Timoshenko beams to a moving force", *J. Sound Vibr.*, **207**(5), 731-742.
Wang, R.T. and Lin, T.Y. (1998), "Random vibration of multi-span Timoshenko beam due to a moving load", *J. Sound Vibr.*, **213**(1), 127-138.
Wang, R.T. and Sang, Y.L. (1999), "Out-of-plane vibration of multi-span curved beam due to moving loads", *Struct. Eng. Mech.*, **7**(4), 361-375.
Wu, J.J., Whittaker, A.R. and Cartmell, M.P. (2000), "The use of finite element techniques for calculating the dynamic response of structures to moving loads", *Comput. Struct.*, **78**(6), 789-799.
Wu, J.S. and Dai, C.W. (1987), "Dynamic responses of multispan nonuniform beam due to movin 0.5 줄g loads", *J. Struct. Eng.*, **113**(3), 458-474.
Xu, H. and Li, W.L. (2008), "Dynamic behavior of multi-span bridges under moving loads with focusing on the effect of the coupling conditions between spans", *J. Sound Vibr.*, **312**(4), 736-753.
Zheng, D.Y., Cheung, Y.K., Au, F.T.K. and Cheng, Y.S. (1998), "Vibration of multi-span non-uniform beams under moving loads by using modified beam vibration functions", *J. Sound Vibr.*, **212**(3), 455-467.
Zhu, X.Q. and Law, S.S. (1999), "Moving forces identification on a multi-span continuous bridge", *J. Sound Vibr.*, **228**(2), 377-396.

Appendix A: Components of the spectral element matrix $\boldsymbol{S}(\omega,l)$

The components of the 4-by-4 spectral element matrix $\boldsymbol{S}(\omega,l)$ are given by (Lee 2009)

$$
\begin{aligned}
s_{11} &= s_{33} = -i\Delta r_t r_e[(e_t^2-1)(e_e^2+1)r_t \\
&\qquad -(e_t^2+1)(e_e^2-1)r_e](k_t r_t - k_e r_e) \\
s_{22} &= s_{44} = -i\Delta(k_t r_t - k_e r_e)[-(e_t^2+1)(e_e^2-1)r_t \\
&\qquad +(e_t^2-1)(e_e^2+1)r_e] \\
s_{12} &= -s_{34} = -\Delta r_t r_e\{(e_t^2-1)(e_e^2-1)(k_t r_e + k_e r_t) \\
&\qquad -[(e_t^2+1)(e_e^2+1)-4e_t e_e](k_t r_t + k_e r_e)\} \\
s_{13} &= -2i\Delta r_t r_e[(e_t^2-1)e_e r_t - (e_e^2-1)e_t r_e](-k_t r_t + k_e r_e) \\
s_{14} &= -s_{23} = 2\Delta r_t r_e(e_t - e_e)(1-e_t e_e)(-k_t r_t + k_e r_e) \\
s_{24} &= -2i\Delta(k_t r_t - k_e r_e)[(e_e^2-1)e_t r_t - (e_t^2-1)e_e r_e]
\end{aligned}
\tag{A1}
$$

where

$$
\begin{aligned}
&\Delta = \frac{EI}{\Phi_1 - \Phi_2} \\
&\Phi_1 = 2r_t r_e\{(e_t^2+1)(e_e^2+1)-4e_t e_e\} \\
&\Phi_2 = (r_t^2+r_e^2)(e_t^2-1)(e_e^2-1) \\
&r_t = k_1^{-1}(k_1^2 - \omega^2\rho A/\kappa GA),\ r_e = k_3^{-1}(k_3^2 - \omega^2\rho A/\kappa GA) \\
&e_t = e^{-ik_1 l},\quad e_e = e^{-ik_3 l}
\end{aligned}
\tag{A2}
$$

where $i=\sqrt{-1}$ is the imaginary unit, and k_1, k_2, k_3 and k_4 are the wavenumbers defined in (Lee 2009).